Intercalibration and Validation of Observations From ATMS and SAPHIR Microwave Sounders

Isaac Moradi, Ralph R. Ferraro, Patrick Eriksson, and Fuzhong Weng

***Abstract*—This paper evaluates the radiometric accuracy of observations from the Advanced Technology Microwave Sounder (ATMS) onboard Suomi National Polar-orbiting Partnership and Sondeur Atmospherique du Profil d' Humidité Intropicale par Radiométrie (SAPHIR) onboard Megha-Tropiques through intercalibration and validation versus *in situ* radiosonde and Global Positioning System Radio Occultation (GPS-RO) observations. SAPHIR and ATMS water vapor channels operate at slightly different frequencies. We calculated the bias due to radiometric errors as the difference between the observed and simulated differences between the two instruments. This difference, which is often referred to as double difference, ranges between 0.3 and 0.7 K, which shows good consistency between the instruments. We used a radiative transfer model to simulate the satellite brightness temperatures (Tbs) using radiosonde and GPS-RO profiles and then compared simulated and observed Tbs. The difference between radiosonde and ATMS Tbs for the middle and upper tropospheric temperature sounding channels was less than 0.5 K at most stations, but the difference between radiosonde and ATMS/SAPHIR Tbs for water vapor channels was between 0.5 and 2.0 K. The larger bias for the water vapor channels is mainly due to several errors in radiosonde humidity observations. The mean differences between the ATMS observations and the Tbs simulated using GPS-RO profiles were 0.2, 0.3, 0.4, 0.2, and −0.2 K for channels 10–14, respectively; and the uncertainty increases from 0.02 K for channel 10 to 0.07 K for channel 14.**

***Index Terms*—Climate change, hydrology, Joint Polar Satellite System (JPSS), microwave, remote sensing, water vapor.**

I. Introduction

MICROWAVE (MW) satellite measurements and derived products play a very important role in weather forecasting, data assimilation, and climate monitoring and assessment. These data are widely used to derive information about key climate variables such as precipitation and atmospheric water vapor and temperature [1]–[5]. MW data are routinely measured by a series of MW instruments onboard polar-orbiting and low-inclination satellites, e.g., Advanced Microwave Sounding Unit-A (AMSU-A), AMSU-B, and the Microwave Humidity Sounder (MHS) onboard the NOAA and MetOp satellites, the Advanced Technology Microwave Sounder (ATMS) on board the Suomi National Polar-orbiting Partnership (S-NPP) and future Joint Polar Satellite System (JPSS) satellites, and Sondeur Atmospherique du Profil d' Humidité Intropicale par Radiométrie (SAPHIR) onboard Megha-Tropiques (M-T).

Spaceborne MW measurements, like any other physical measurements, are subject to errors and uncertainties, which can be classified into radiometric and geometric errors [6]. Radiometric errors, which are the focus of this paper, are caused by several sources, including drift in sensor calibration, imperfect antenna and local electronics, radio-frequency interference, reflector emissivity, uncertainty in the warm and cold (space-view) load temperatures, and nonlinearity in the calibration. Due to the lack of reference measurements for validating MW observations, alternative methods are used to quantify the radiometric errors in MW measurements. These methods include validation using airborne observations [7], intercalibration with similar spaceborne instruments [8]–[10], intercomparison with forward calculations using a radiative transfer model and atmospheric state variables from radiosonde [3], Numerical Weather Prediction (NWP) model fields, or Global Positioning System Radio Occultation (GPS-RO) [11].

Intercomparing observations from similar spaceborne instruments is one of the methods that have been extensively used to identify relative differences between the instruments and allow for proper usage of their measurements and derived products, particularly for developing long-term records for climate applications [8], [9]. In this case, one of the instruments that are stable over time in terms of its performance and minimal orbital drift is chosen as the reference, and other (target) instruments are intercalibrated with respect to the reference instrument. Intercalibration requires that both target and reference instruments observe the same location as close in time as possible. Intersatellite differences are normally scene dependent; thus, the coincident observations should cover a wide range of atmospheric and surface conditions. However, most of the collocations from sun-synchronous polar-orbiting satellites occur at high latitudes, where the observed brightness temperatures (Tbs) are normally low. Therefore, intercalibration of MW instruments onboard polar-orbiting satellites has always been challenging. The low-inclination non-sun-synchronous satellites, e.g., the M-T satellite, yield numerous collocations with sun-synchronous polar-orbiting satellites, e.g., the S-NPP

Manuscript received October 16, 2014; revised February 4, 2015; accepted April 16, 2015. This work was supported by the National Oceanic and Atmospheric Administration under Grant NA09NES4400006 (Cooperative Institute for Climate and Satellites) at the Earth System Science Interdisciplinary Center, University of Maryland.

I. Moradi is with the Cooperative Institute for Climate and Satellites, Earth System Science Interdisciplinary Center, University of Maryland, MD 20740 USA, and also with the Joint Center for Satellite Data Assimilation, National Oceanic and Atmospheric Administration, College Park, MD 20740 USA (e-mail: Isaac.Moradi@noaa.gov).

R. R. Ferraro and F. Weng are with the Center for Satellite Applications and Research, National Environmental Satellite, Data, and Information Service, National Oceanic and Atmospheric Administration, College Park, MD 20740 USA.

P. Eriksson is with the Department of Earth and Space Sciences, Chalmers University of Technology, 41296 Gothenburg, Sweden.

Color versions of one or more of the figures in this paper are available online at http://ieeexplore.ieee.org.

Digital Object Identifier 10.1109/TGRS.2015.2427165

0196-2892 © 2015 IEEE. Personal use is permitted, but republication/redistribution requires IEEE permission.
See http://www.ieee.org/publications_standards/publications/rights/index.html for more information.

satellite, in the tropical region and offer more opportunities for direct time and space collocations. Nevertheless, intercomparing similar instruments only reveals the relative differences between the instruments and cannot be used to identify the absolute errors in the measurements. Other methods that can be employed to validate the MW satellite observations include intercomparing satellite observations with Tbs simulated using radiosonde and GPS-RO profiles and a radiative transfer model. However, both the radiosonde and GPS-RO data, as well as radiative transfer (RT) calculations, are subject to errors and uncertainties that affect the reliability of the results.

ATMS and SAPHIR are MW sounding instruments flying onboard the S-NPP and M-T satellites, respectively. ATMS provides information about both atmospheric water vapor and temperature [12], [13], but SAPHIR is only equipped with water vapor channels operating near the water absorption line at 183 GHz and provides information about the distribution of tropospheric water vapor in the tropical region [14]. Although these instruments are well calibrated and tested before launch, they require extensive postlaunch assessment and validation due to possible drift in calibration. This paper focuses on intercomparing observations from similar water vapor channels on the SAPHIR and ATMS instruments, validating SAPHIR and ATMS water vapor, as well as ATMS middle and upper tropospheric temperature sounding channels using radiosonde data, and validating ATMS upper tropospheric and stratospheric temperature sounding channels using GPS-RO profiles.

The remainder of this paper is organized as follows. Section II introduces data and satellite instruments, Section III discusses the methodology and collocation criteria, Section IV presents the results and findings of this study, and Section V summarizes this study.

II. Data and Instruments

A. ATMS and SAPHIR Instruments

ATMS is a cross-track MW sounder with 22 channels operating at MW frequencies from 23.8 to 190.31 GHz. ATMS is currently flying on the S-NPP satellite and is planned to fly on the U.S. next-generation polar-orbiting operational environmental satellite system named Joint Polar Satellite System (JPSS). S-NPP, which was launched in October 2011, is in a sun-synchronous orbit, an altitude of 824 km, and an inclination of 97.1°, yielding an orbital period of 101 min, with the ascending equatorial crossing time at 01:30 P.M. local time [15]. The ATMS characteristics, including frequency, bandwidth, beamwidth, and the noise equivalent temperature difference (NEΔT), are reported in Table I.

Weighting functions, which show the sensitivity of the ATMS channels to different altitudes of the atmosphere, are shown in Fig. 1. In this paper, we used ATMS Sensor Data Records, which are corrected for the antenna pattern and converted to Tb in kelvins [12], [16], [17].

M-T, which was launched in November 2011, is a low-inclination satellite with an altitude of 865 km and an inclination of 19.98°, yielding an orbital period of 101 min. This means that the satellite only visits the tropical band between 30 S and 30 N. There are primarily two MW instruments onboard M-T: the Microwave Analysis and Detection of Rain and Atmospheric Systems (MADRAS) and SAPHIR. The MADRAS instrument, whose primary purpose was to measure atmospheric temperature, surface properties, and precipitation, experienced several malfunctions and is not operating at present; thus, SAPHIR is currently the only operational MW instrument on board the M-T satellite. The characteristics of the channels of SAPHIR are shown in Table II. All SAPHIR channels have horizontal polarization, the swath width is 1700 km, and the resolution is 10 km at nadir for all the channels. As shown, the SAPHIR and ATMS channels operate at slightly different frequencies, and SAPHIR also has a few additional water vapor channels. Weighting functions for the SAPHIR channels are also shown in Fig. 1. We used the SAPHIR L1A data that are processed by Centre National d'Etudes Spatiales. SAPHIR data are not corrected for the antenna pattern, but because of the high beam efficiency, the effect of antenna pattern correction is negligible for the water vapor channels [17].

TABLE I
ATMS Radiometric and Channel Characteristics. BDW Indicates the Bandwidth in Megahertz. BMW Indicates the Beamwidth in Degrees. Ant Indicates the Antenna, Frequency Is in Gigahertz, and NEΔT Is in Kelvins [15]

Chan.	Frequency	BDW	NEΔT	BMW	Pol.	Ant
1	23.80	270	0.5	5.2	V	A
2	31.40	180	0.6	5.2	V	A
3	50.30	180	0.7	2.2	H	A
4	51.760	400	0.5	2.2	H	A
5	52.80	400	0.5	2.2	H	A
6	53.596±0.115	170	0.5	2.2	H	A
7	54.40	400	0.5	2.2	H	A
8	54.94	400	0.5	2.2	H	A
9	55.50	330	0.5	2.2	H	A
10	57.290344 [f0]	330	0.75	2.2	H	A
11	f0±0.217	78	1.0	2.2	H	A
12	f0±0.322±0.048	36	1.0	2.2	H	A
13	f0±0.322±0.022	16	1.5	2.2	H	A
14	f0±0.322±0.010	8	2.2	2.2	H	A
15	f0±0.322±0.0045	3	3.6	2.2	H	A
16	88.20	2000	0.3	2.2	V	B
17	165.50	3000	0.6	1.1	H	B
18	183.31±7.0	2000	0.8	1.1	H	B
19	183.31±4.5	2000	0.8	1.1	H	B
20	183.31±3.0	1000	0.8	1.1	H	B
21	183.31±1.8	1000	0.8	1.1	H	B
22	183.31±1.0	500	0.9	1.1	H	B

B. GPS-RO Observations

GPS-RO observations signify the radio signals transmitted by the GPS satellites measured by a receiver on a low Earth orbiting (LEO) satellite. GPS-RO measurements represent the atmosphere between the GPS satellite and the LEO satellite, and a series of such measurements are organized in one profile. The primary measurement is the delay (phase) of the signal due to refraction by the atmosphere between the GPS and the LEO during the occultation. However, these raw measurements cannot be directly used in many applications. Therefore, the time delay is converted to the bending angle of the signal. The bending angle then is transformed into refractivity using the Abel transformation. Finally, the refractivities are transformed into atmospheric products of temperature, humidity, and pressure using *a priori* profiles and the hydrostatic equilibrium concept.

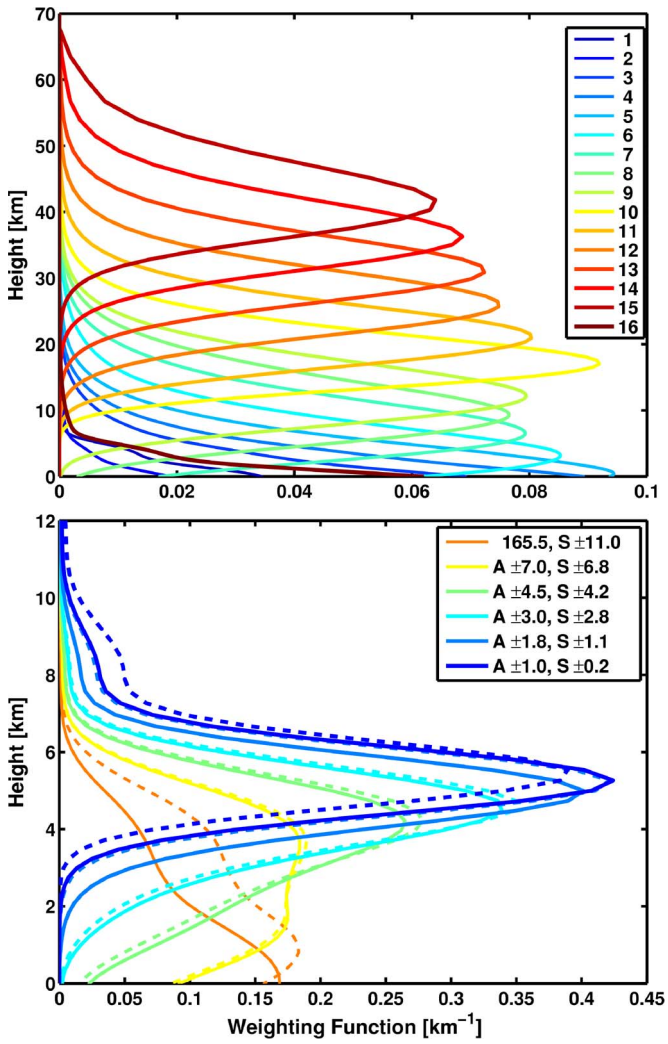

Fig. 1. Temperature weighting functions for the ATMS and SAPHIR channels. (Top) ATMS channels 1–16. (Bottom) (solid lines) ATMS and (dashed lines) SAPHIR water vapor channels. The legend for the bottom plot shows the passbands with respect to 183.31 GHz (A±# for ATMS and S±# for SAPHIR) and correspond to channels 17–22 for ATMS and S6–S1 for SAPHIR, respectively.

The refractivity N is related to atmospheric pressure P (mbar), temperature T (kelvin), and humidity as follows:

$$N = (n-1) \times 10^6 = 77.6\frac{P}{T} + 3.73 \times 10^5 \frac{P_w}{T^2} + 4.03 \times 10^7 \frac{n_e}{f^2} + 1.4W \quad (1)$$

where P_w is the partial pressure of water vapor in millibars, n_e is the electron number density, f is the transmission frequency in hertzs, and W is the liquid water content in grams per cubic meter. These terms are referred to as the dry, wet, ionospheric, and scattering terms [18]. The dry term is the most significant term from the upper troposphere to the upper stratosphere.

The raw measurements of time delay are very accurate and stable from the middle troposphere to the lower stratosphere, extending roughly from 5 to 25 km [19], [20]. However, outside this range, the GPS-RO data are affected by several errors, including superrefraction in the lower troposphere [21], [22], residual ionospheric effect, and the Abel high-altitude initialization above 25 km [19], [23]. In this paper, we used the GPS-RO data from the Constellation Observing System for Meteorology, Ionosphere, and Climate, which have been available from six LEO satellites since 2006. We used the GPS-RO wet profiles available from the University Corporation for Atmospheric Research.

TABLE II
SAPHIR RADIOMETRIC AND CHANNEL CHARACTERISTICS [39]

Chan.	Frequency	Bandwidth	NEDT
S1	183.31±0.20	200	2.35
S2	183.31±1.10	350	1.45
S3	183.31±2.80	500	1.36
S4	183.31±4.20	700	1.38
S5	183.31±6.80	1200	1.03
S6	183.31±11.0	2000	1.10

C. Radiosonde Data

The Atmospheric Radiation Measurement (ARM) Climate Research Facility is a global change research program, which has been supported by the U.S. Department of Energy since 1989. In this paper, we used the radiosonde data from the following ARM stations: the Tropical Western Pacific stations (TWP-C1, TWP-C2, and TWP-C3) located in Manus Island (Papua New Guinea), Nauru Island (the Republic of Nauru), and Darwin (Australia), respectively; and Southern Great Plains (SGP-C1) located in Lamont (Oklahoma, USA) [24], [25]. The ARM stations are equipped with Vaisala RS92 sensors for measuring relative humidity. While RS92 is one of the most reliable sensors, several errors are involved in the measurements, including daytime radiation dry bias and contamination errors. Because of the large magnitude of the daytime radiation bias [26], [27], we only used nighttime data that normally extend from the ground to about 20 km.

III. INTERCOMPARISON METHOD

This study includes three steps: 1) intercomparing similar water vapor channels on ATMS and SAPHIR; 2) evaluating observations from ATMS and SAPHIR water vapor channels and ATMS middle and upper tropospheric temperature sounding channels versus radiosonde data; and 3) evaluating observations from ATMS upper tropospheric and stratospheric temperature sounding channels versus GPS-RO profiles. The last two steps are conducted by simulating ATMS and SAPHIR Tbs using the Community Radiative Transfer Model (CRTM) [28].

A. Collocation Criteria

Intercalibrating satellite observations from two different platforms and, likewise, evaluating satellite observations using *in situ* radiosonde and GPS-RO profiles require careful matching between the observations. In the case of collocating the ATMS and SAPHIR observations, the two instruments have different characteristics and geometries, as was previously described. S-NPP and M-T produce a lot of coincident observations because the overpass times for S-NPP and M-T are not synchronized, but because of difference in the geometry, most of the collocations cannot be used for intercomparison. Therefore, we

limited the collocations to nadir observations to ensure that both satellites observe the same target with the same geometry. Since true nadir observations do not exist for either of the instruments, we only used the subnadir beam positions for the intercomparison. Other collocation criteria were a time difference of less than 1 h and a spatial distance of less than 50 km. However, as it is explained later, these thresholds are not very critical in our study, because SAPHIR and ATMS collocations occur in the tropical region, where the diurnal variation of satellite Tbs is small.

In the case of collocating satellite and radiosonde or GPS-RO profiles, it is required to take into account that satellite data are area averaged, whereas radiosonde data are point measurements and GPS-RO data are limb-sounding measurements. Both radiosonde and GPS-RO profiles drift with altitude. The drift in radiosonde profiles is estimated to be around 50 km, but highly depends on the wind speed and balloon burst altitude. The drift in GPS profiles depends on the geometry of GPS and LEO orbits and is discussed in Section IV.

Because of the drift in the profiles, it is not possible to collocate sonde and GPS profiles with an individual satellite footprint; therefore, we collocated each profile with all the satellite footprints within a target area with a radius of 50 km. It should be noted that, in the case of collocating satellite observations with radiosonde or GPS-RO profiles, restricting the collocations to nadir-only satellite observations will greatly reduce the number of collocations. Therefore, we should take into account satellite observations from all the beam positions. In this case, radiative transfer models can simulate Tbs for the corresponding Earth incidence angles.

In addition, satellite observations are subject to cloud effects, even at MW frequencies, whereas the Tbs simulated using a radiative transfer model are simulated for clear-sky conditions. Thus, it is required to filter out the cloud-contaminated observations before conducting the collocation. Due to the natural lapse rate in temperature, the Tbs for the channels sensitive to higher altitudes of the atmosphere are lower than the Tbs for the channels sensitive to the lower altitudes. In the presence of optically thick clouds, the Tbs for the upper channels become either very close or even greater than the Tbs for the lower channels [29]–[31]. We used ice water path (IWP) data retrieved from ground cloud radar and satellite MW measurements [32] to develop the cloud filters for ATMS and SAPHIR. The cloud screening method developed here is very similar to that reported for AMSU, e.g., [29] and [31], but we examined the thresholds independently. Generally, the difference between Tbs for a channel sensitive to lower troposphere and a channel sensitive to upper troposphere is utilized as the cloud filter. In this paper, 183 ± 1 (Tb1) and 183 ± 7 (Tb7) are employed as upper and lower tropospheric channels, respectively. Fig. 2 shows the difference between Tb1 and Tb7, i.e., $\Delta\mathrm{Tb} = \mathrm{Tb1} - \mathrm{Tb7}$, as a function of IWP values. As shown, the observations are almost independent of IWP as long as $\Delta\mathrm{Tb}$ is less than -15 K; then, $\Delta\mathrm{Tb}$ increases with IWP. Fig. 2 also shows the relation between Tb1 and IWP. Tb1 is normally larger than 240 K under clear-sky conditions or in the presence of thin clouds and then decreases with IWP. We used a threshold of 240 K for Tb1 so that the pixel is determined to be cloud free if $\Delta\mathrm{Tb} < -15$ K and $\mathrm{Tb1} >$ 240 K. Both thresholds were determined using RT calculations. Some of the observations that are associated with very low IWP are also screened out by the Tb1 filter. It is possible to choose a lower threshold for Tb1 to avoid this, but we decided to use the threshold determined by the RT calculations. The cloud-free observations for SAPHIR can be determined using similar channels, i.e., 183 ± 1.1 for Tb1 and 183 ± 6.8 for Tb7. The thresholds are also valid for the SAPHIR channels. MW temperature sounding channels operate at a frequency of 50–60 GHz (a wavelength λ of 6–5 mm). Significant scattering occurs only if particles have a size that is of the same order as the wavelength. Thus, the temperature sounding channels that operate at low frequencies, with a very large wavelength, are not as sensitive as water vapor channels to clouds, but primarily to larger hydrometers such as snow and hail [33]. In addition, these channels peak at altitudes higher than where precipitating clouds form; thus, the impact of precipitating clouds on these channels is minimal. Therefore, we did not apply any cloud filter to data from temperature sounding channels. In summary, collocating *in situ* radiosonde and GPS-RO data with satellite measurements require four criteria: the time difference between the measurements, the spatial distance between the measurements, the size of the target area, and the cloud screening for the satellite data from water vapor channels.

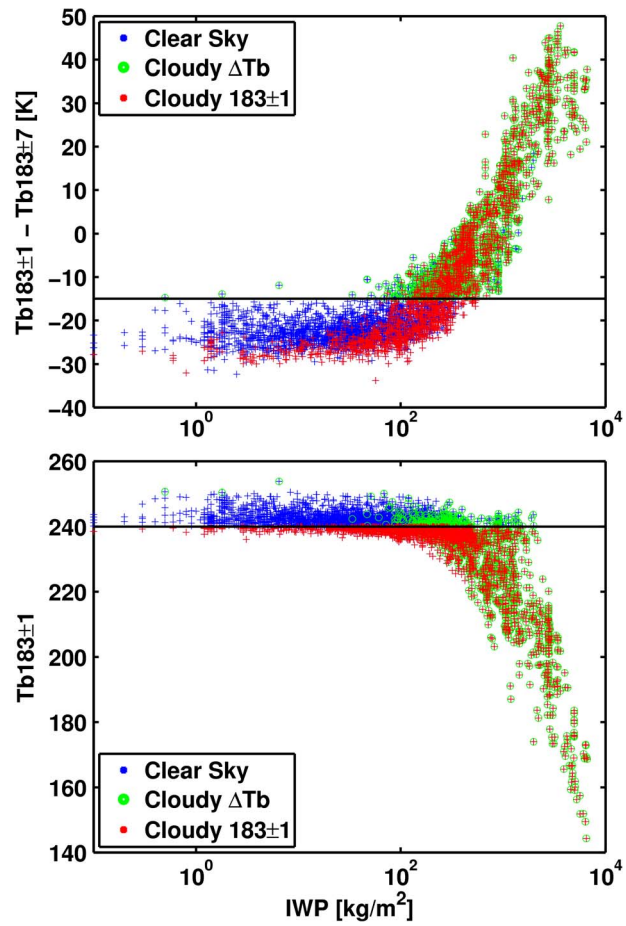

Fig. 2. Relation between (top) IWP and $\Delta\mathrm{Tb} = \mathrm{Tb1} - \mathrm{Tb7}$ and (bottom) IWP and ATMS Tbs from channel 1. The legend shows the data that are considered either clear or cloudy by one of the filters.

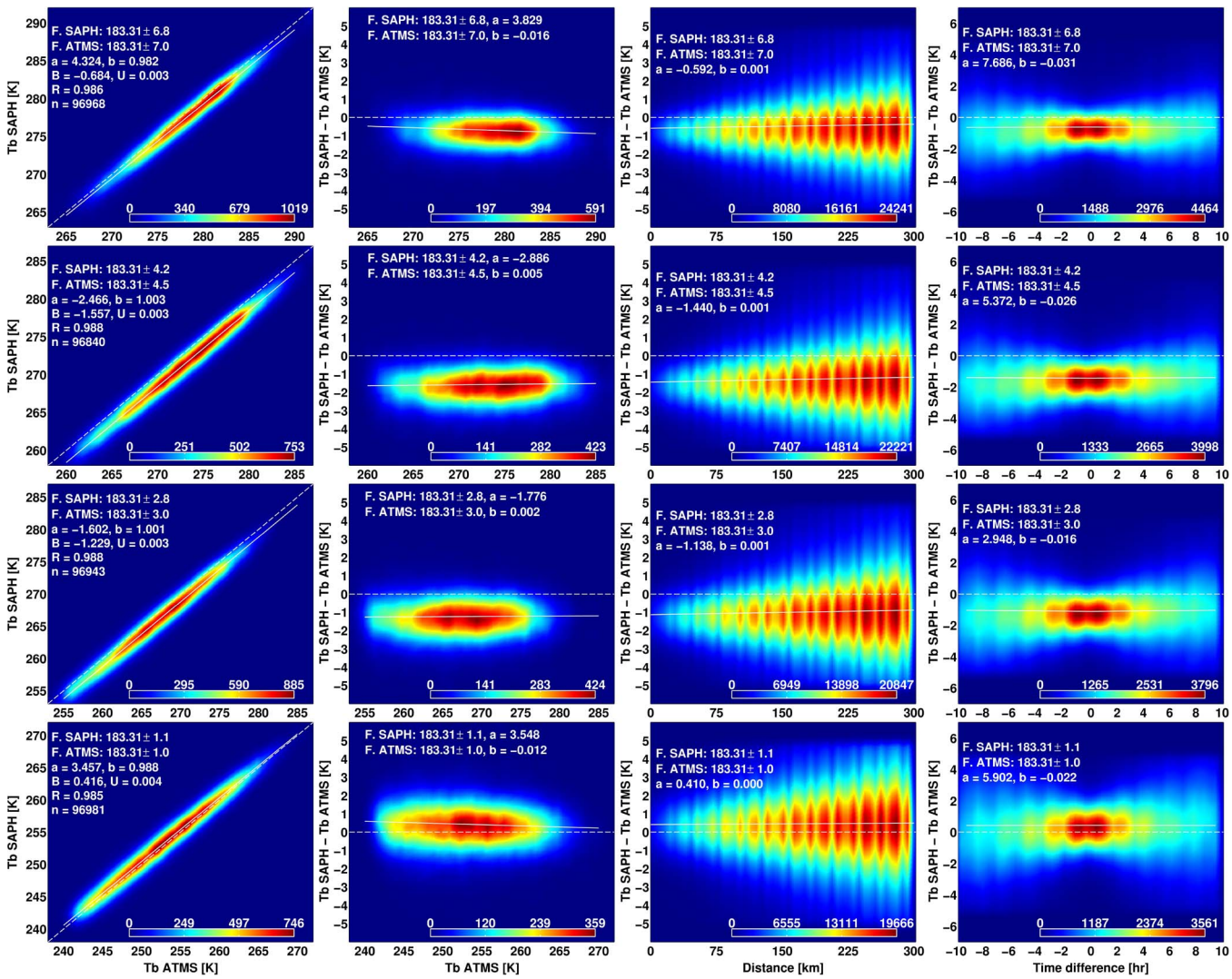

Fig. 3. Collocated SAPHIR and ATMS observations. Rows indicate results for different channels (frequencies of both ATMS and SAPHIR channels are printed on the plots). The first column shows SAPHIR Tbs versus collocated ATMS Tbs, and the second to fourth columns show the difference between the SAPHIR and ATMS Tbs (SAPHIR minus ATMS) as a function of ATMS Tb (scene temperature), the distance between the collocated SAPHIR and ATMS data, and the time difference between the collocated SAPHIR and ATMS data, respectively. F indicates frequency of the channels, a and b indicate the offset and slope of the fitted line, B indicates the mean difference between the SAPHIR and ATMS Tbs in kelvins, U indicates the uncertainty of the bias in kelvins, R indicates the correlation coefficient, and n indicates the number of collocations.

IV. Results

Here, we first discuss the results for intercomparing the SAPHIR and ATMS water vapor channels and then compare the SAPHIR and ATMS water vapor channels and the ATMS middle and upper tropospheric temperature sounding channels versus ARM radiosonde data. Finally, we validate the ATMS upper tropospheric and stratospheric temperature sounding channels using GPS-RO data. We used the data for the period of January 2012 to October 2013.

A. Intercomparing SAPHIR and ATMS Observations

We first collocated the ATMS and SAPHIR observations in clear-sky conditions, with a time threshold of 1 h and a spatial threshold of 50 km. Fig. 3 shows the comparison between the collocated ATMS and SAPHIR observations. The frequencies of the ATMS and SAPHIR channels and the statistics for the comparison are indicated on the plots. As shown, the mean differences (bias) between the ATMS and SAPHIR observations are −0.7, −1.6, −1.2, and 0.4 K for the lower to upper channels, respectively. The statistical uncertainty of the bias is negligible in all cases. The correlation coefficients between the SAPHIR and ATMS observations are greater than 0.98 for all the channels. The slope of the fitted line ranges between 0.98 and 1.0, which is very close to unity. Because of the frequency difference between the SAPHIR and ATMS channels, the weighting functions of the similar channels peak at slightly different altitudes, which introduces a systematic difference between the observations of the two instruments. Therefore, the difference between the ATMS and SAPHIR observations (D_O) is due to both radiometric errors and frequency mismatch. The difference due to frequency mismatch should not be taken as a bias in the observations. This difference was estimated by simulating the ATMS and SAPHIR Tbs using a subset of randomly selected ARM radiosonde profiles and the CRTM model and then subtracting the simulated Tbs from each other

TABLE III
OBSERVED AND SIMULATED DIFFERENCES BETWEEN ATMS, SAPHIR, AND MHS MEASUREMENTS. D_O AND D_S INDICATE SAPHIR MINUS ATMS OBSERVATIONS AND SIMULATIONS, RESPECTIVELY. S-A INDICATES THE DOUBLE DIFFERENCE ($D_O - D_S$) FOR SAPHIR AND ATMS, S-M INDICATES THE DOUBLE DIFFERENCE FOR SAPHIR AND MHS, AND M-A INDICATES THE DIFFERENCE BETWEEN THE MHS AND ATMS INSTRUMENTS

ATMS	SAPHIR	D_o	D_s	S-A	S-M	M-A
183±7.0	183±6.8	-0.68	-0.42	-0.26	+0.20	-0.46
183±4.5	183±4.2	-1.56	-0.91	-0.65		
183±3.0	183±2.8	-1.23	-0.93	-0.30	-0.45	+0.15
183±1.0	183±1.1	+0.42	+0.90	-0.48	-0.09	-0.39

(D_S). Finally, the difference between D_O and D_S, which can be counted as a double difference, shows the bias due to radiometric errors. The aforementioned statistics, i.e., D_O, D_S, and double difference, are reported in Table III. As shown, the double difference ranges from -0.3 to -0.7 K for different channels, which shows a very good agreement between the two instruments.

The double differences (SAPHIR minus ATMS) are negative for all the channels, which means that the SAPHIR measurements are systematically lower than the ATMS measurements. However, these systematic differences should not be attributed to a larger radiometric error in one of the instruments unless they can be independently justified. We employed a third instrument, i.e., the MHS instrument onboard NOAA-19, to further investigate this systematic difference. The double differences between the SAPHIR and MHS measurements, similar to the double differences for the SAPHIR and ATMS measurements, are shown in Table III. MHS has three water vapor channels operating at 183 ± 1, 183 ± 3, and 183 ± 7 GHz , but it does not have any channel at 183 ± 4.5 GHz. Therefore, the statistics are not shown for that specific channel. The results show that only SAPHIR S3 has a negative bias relative to MHS. Although the difference between SAPHIR S2 and the corresponding channel on MHS is negative, the difference is small and negligible. However, SAPHIR S5 has a positive bias ($+0.2$ K) relative to the corresponding channel on MHS. The difference between the double differences of SAPHIR relative to the ATMS and MHS instruments, i.e., [SAPHIR - ATMS] - [SAPHIR - MHS], can be counted as the difference between MHS and ATMS. As shown in Table III, ATMS channels 18 and 22 have a cold bias relative to corresponding channels on MHS, but ATMS channel 20 has a warm bias relative to MHS. The results, with mixed positive and negative double differences, show the sensitivity of the intercalibration to the reference instrument. In addition, employing SAPHIR measurements to calculate the differences between the MHS and ATMS instruments indicates a great application of double differences using measurements from low-inclination satellites to transfer calibrations among the polar-orbiting satellites.

Fig. 3 also shows the mean difference between the ATMS and SAPHIR Tbs as a function of ATMS Tb, temporal difference, and spatial distance between the collocations. The slope of the fitted line between the intersatellite differences and the ATMS Tbs can be up to 0.02, which means that the scene dependence of the differences between the two instruments can be up to about 2 K per 100-K change in the scene temperature.

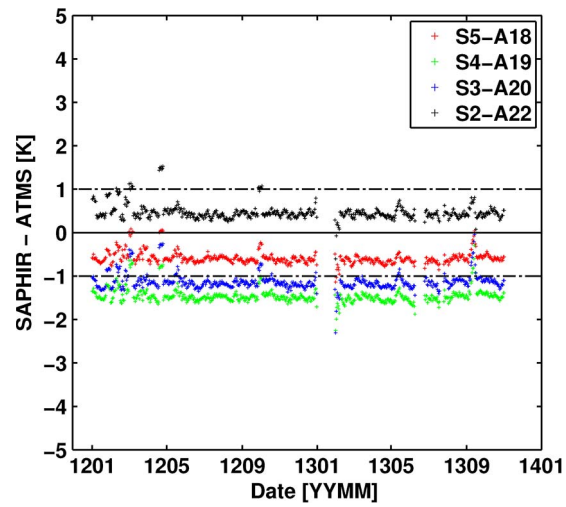

Fig. 4. Time series of the weekly moving averages of differences between the SAPHIR and ATMS measurements. In the legend, S indicates the SAPHIR channel number, and A indicates the corresponding ATMS channel.

This indicates that the scene dependence of the intercalibration coefficients is important and should be taken into account when intercalibrating MW instruments. However, the mean difference does not show any significant relation with temporal difference and spatial distance. For instance, a 50-km spatial distance would only introduce less than 0.05-K error, since the slope of the fitted line between distance and the differences is up to $0.001\ \mathrm{K} \cdot \mathrm{km}^{-1}$, and a 1-h time difference would only introduce less than 0.03-K bias because the slope of the fitted line is $0.03\ \mathrm{K} \cdot \mathrm{hr}^{-1}$ for the time difference. However, the standard deviation of the differences between ATMS and SAPHIR significantly increases with spatial distance, as might be expected, ranging from 2 to 8 K over distances of 50–300 km. The sensitivity to changes in time is not very critical, with only a slight increase in the standard deviation. It should be noted that these results are only valid in the tropical region due to negligible diurnal variation of temperature and humidity, and the results should not be extended to the regions outside the tropical region.

Fig. 4 shows the time series of the weekly moving averages of differences between the SAPHIR and ATMS measurements. The differences between the two instruments are very stable and only show some small fluctuations. The time series is almost for two years, thus not enough for evaluating the seasonal dependence or trends in the differences between the two instruments. Seasonal dependence can be introduced by either seasonal change in the diurnal variation of Tbs or seasonal variation in the regime of the convective clouds since those clouds have a significant effect on the water vapor channels. However, in the tropical region, the diurnal variation is very small and may only slightly change with season. We also used a small time threshold, which will eliminate the impact of a small diurnal variation on the intercomparison results. In addition, we screened out the cloud-contaminated observations from the analysis. Thus, the intercomparison results are not expected to have any seasonal dependence even if a longer period of data is used for intercomparison.

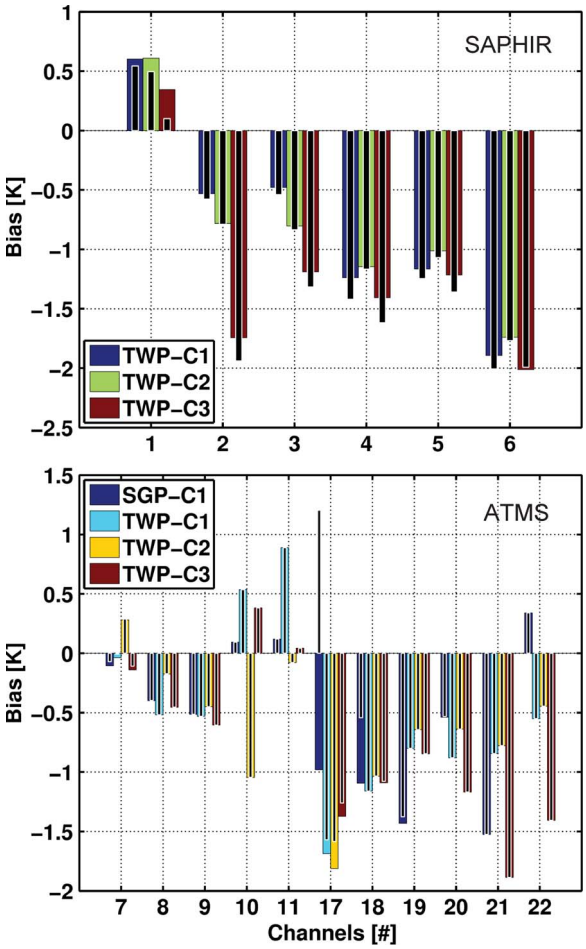

Fig. 5. Mean difference between the SAPHIR/ATMS Tbs and the Tbs simulated using ARM radiosonde profiles. The color bars indicate the bias with respect to the ARM Tbs simulated using land emissivity, and the black bars indicate the bias with respect to the ARM Tbs simulated using ocean emissivity. The top panel is for the SAPHIR channels, where the x labels 1–6 indicate the SAPHIR S1–S6 channels, respectively. The bottom panel is for ATMS, where the x labels show the ATMS channels' number.

B. Comparison With Radiosonde Data

Fig. 5 shows the bias for both the SAPHIR and ATMS observations versus simulated Tbs using CRTM and ARM radiosonde profiles. The figure shows the bias with respect to Tbs simulated using both land and ocean emissivity. Since MW surface emissivity, particularly over land, is not well known for these frequency ranges, this is particularly useful to see whether the bias is affected by the surface emissivity. Fig. 5 only shows the ATMS temperature sounding channels that are sensitive to middle and upper troposphere and the water vapor channels for both SAPHIR and ATMS instruments. The bias for the lower tropospheric and window channels of ATMS is largely influenced by the surface emissivity. In addition, radiosonde profiles only reach up to about 20 hPa; thus, the simulated Tbs for stratospheric channels, which are sensitive to altitudes outside the range of sonde profiles, are not reliable and show very large biases. Therefore, we excluded the channels whose weighting functions peak either in lower troposphere near the surface or above the tropopause. Fig. 5 shows that, for the channels that are sensitive to middle to upper troposphere, the difference between the land and ocean biases is very small, indicating that the statistics are not affected by the surface emissivity. The TWP stations are located in the tropical region where total precipitable water is very high; thus, the weighting functions of the water vapor channels peak at high altitudes, and the measurements are almost insensitive to the surface. However, the Southern Great Plains station that is located at midlatitudes shows a large surface contribution for ATMS channels 17 and 18, which can be seen in the differences between land and ocean biases. TWP-C3 shows very large biases for SAPHIR channel 2 and ATMS channels 21 and 22. This large bias is not related to the surface contribution, because the differences between the land and ocean biases are very small. The bias is unlikely to be due to error in satellite data since other stations do not show such a large bias for those channels. Therefore, the large difference is likely to be due to error in sonde data. The results for the water vapor channels are consistent with those of Clain *et al.* [34], who reported a difference of less than 2 K between SAPHIR and forward calculations using radiosonde data.

Overall, the bias is smaller for the temperature sounding channels than for the water vapor channels, which is mainly because the radiosonde temperature measurements have better accuracy than the sonde humidity measurements [26], [35], [36]. Previous studies have generally reported a dry bias for Vaisala radiosonde sensors, e.g., [3] and [36]. The dry bias in sonde data is translated into larger simulated Tbs for the water vapor channels. The overall result of the radiosonde dry bias is that the observed Tbs are systematically lower than the simulated Tbs. The amount of the sonde dry bias depends on many factors such as atmospheric state variables, for instance, the bias is larger in dry conditions than in moist conditions, and radiosonde sensor, but it is generally estimated to be between 0.5 and 1.5 K for Vaisala RS92 sensors [27], [36], [37]. If we subtract this bias from the difference between the satellite Tbs and the radiosonde simulated Tbs, then the remaining bias in the water vapor channels is around 1 K, which is relatively consistent with the intercalibration results. It should be noted that this remaining difference may be due to either radiometric error in the ATMS and SAPHIR observations or sampling (temporal and spatial) mismatch between the collocations. Although the sampling mismatch is expected to be random and cancel out when comparing radiosonde and satellite data, ARM radiosonde data used in this study are normally collected at 12:00 and 24:00 UTC, and the satellite overpass time is almost fixed in terms of local time. Therefore, the satellite will always pass over the radiosonde stations either before or after sonde launch time. In addition, it normally takes more than 1 h for radiosonde to reach 20 km, whereas the satellite observations are integrated in less than a second. Thus, there will be always some residual time difference between radiosonde and satellite observations. Despite all the aforementioned limitations, radiosonde data are still very valuable for validating MW water vapor channels. In addition to the radiosonde dry bias and sampling errors, the RT calculations are also subject to errors and uncertainty, such as error in spectroscopic databases, and line shapes, but these errors are estimated to be small [35].

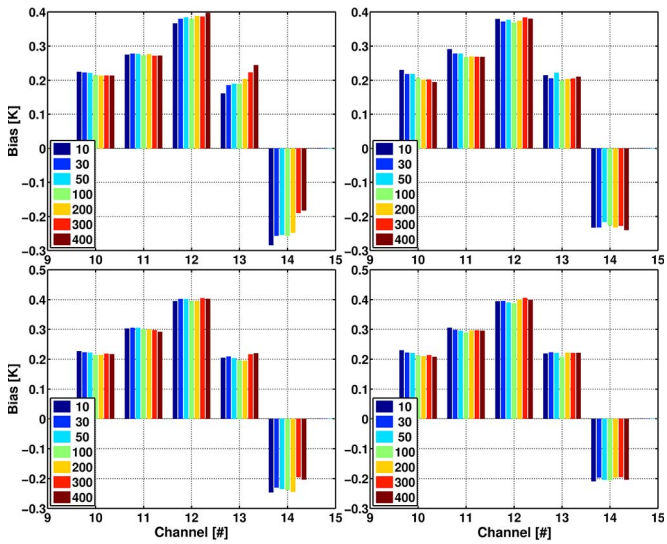

Fig. 6. Mean difference between the ATMS and GPS-RO Tbs. The time difference threshold was 30 min for the first row and 60 min for the second row. The spatial distance threshold was 50 km for the first column and 100 km for the second column. The legend indicates the altitude (in hPa) where GPS coordinates were used for collocation.

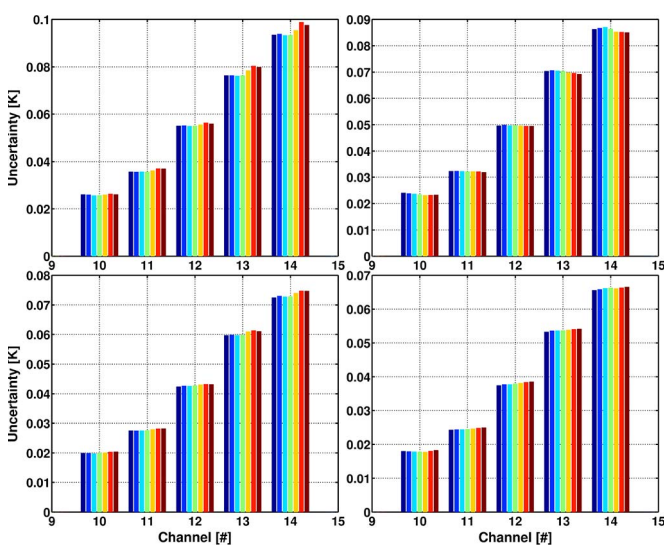

Fig. 7. Same as Fig. 6, but for the statistical uncertainty of the mean difference between GPS-RO and ATMS.

C. Comparison With GPS-RO Data

Fig. 6 shows the mean difference between the ATMS Tbs and the Tbs simulated using GPS-RO data. The corresponding uncertainties, which are defined as standard deviation over the square root of the number of collocations, are shown in Fig. 7. In order to investigate the effect of temporal and spatial thresholds on the bias and uncertainty, both statistics were calculated using different thresholds. We used two different temporal (30 and 60 min) and two different spatial (50 and 100 km) thresholds. The results are shown in Figs. 6 and 7 for bias and uncertainty, respectively. Obviously, the bias does not significantly depend on the spatial and temporal thresholds. The uncertainty of the bias slightly decreases when the temporal and spatial thresholds are changed from 30 to 60 min and from 50 to 100 km, respectively; but that is mainly due to increase in number of collocations. In addition,

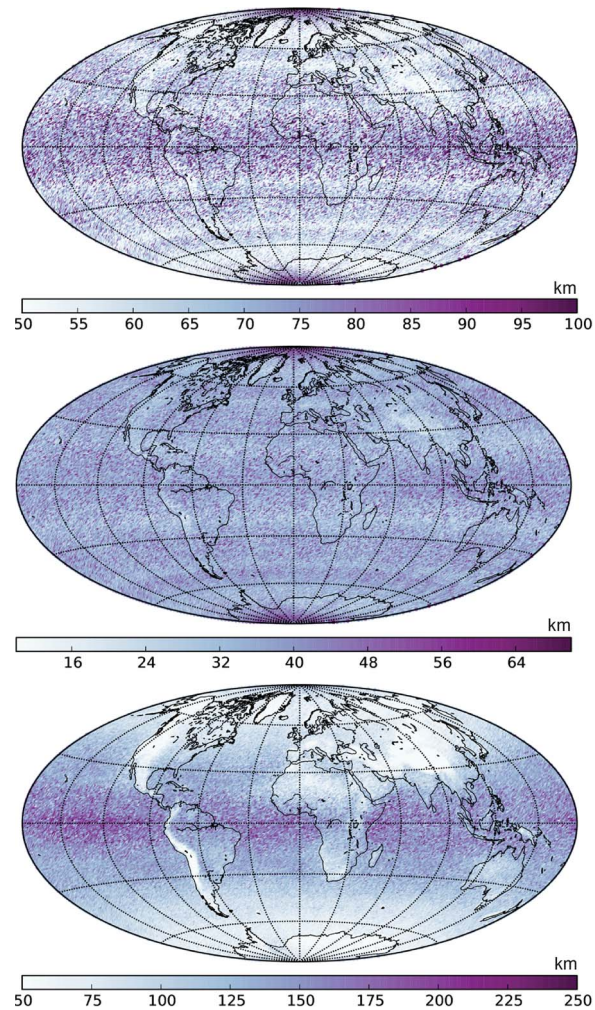

Fig. 8. Drift in GPS profiles at different altitudes. (Top) Drift from 400 to 10 hPa. (Middle) Drift from 400 to 100 hPa. (Bottom) Drift from ground to 400 hPa. The legends show the drift in kilometers.

one of the concerns for collocating GPS-RO and satellite observations is that GPS-RO profiles drift with altitude. In order to investigate the impact of the drift on the statistics, we collocated satellite observations with GPS-RO location at different altitudes. The statistics calculated based on different GPS-RO locations are also shown in Figs. 6 and 7. The uncertainty of the bias does not depend on the GPS-RO location that is used for collocation. However, the bias for channels 13 and 14 slightly depends on the GPS-RO location when the temporal and spatial thresholds are small. This is likely to be due to limited number of collocations. Otherwise, the bias is independent of the GPS-RO location that is used for collocation. This can be explained by either a nonsignificant drift in the GPS-RO profiles or the homogeneity of the upper tropospheric and stratospheric temperatures. Fig. 8 shows the drift in GPS-RO profiles from ground to 400 hPa and the drift from 400 to 100 and 10 hPa. As shown, the drift from ground to 400 hPa depends on the latitude and changes from more than 200 km in the tropical region to less than 100 km at midlatitude and high latitude. Although this drift is significant, at least in the tropical region, it is not important for validating satellite data using GPS-RO observations because the temperature sounding channels that are validated using GPS-RO

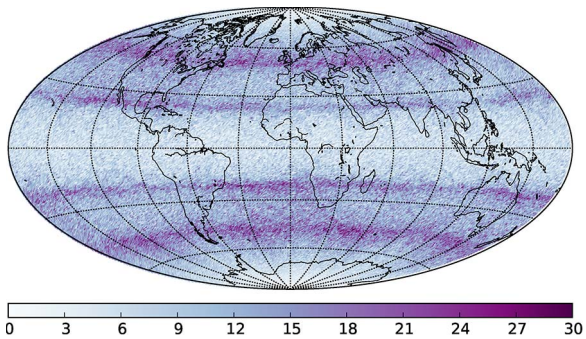

Fig. 9. Spatial distribution of the number of GPS-RO profiles.

profiles are not sensitive to this layer. In addition, as shown in Fig. 9, most of the GPS-RO observations are from midlatitude and high latitude, where the drift is not very large. The drift from 400 to 100 hPa is mostly less than 40 km and does not show any changes with latitude. The drift from 400 to 10 hPa only slightly depends on the latitude and changes from about 80 km over the tropical region to less than 60 km at midlatitude and high latitude. The drift from 400 to 10 hPa seems large over the tropical region, but as aforementioned, most of GPS-RO observations are from midlatitude and high latitude (see Fig. 9).

It is worth looking closer at the statistics that are computed using a temporal threshold of 60 min and a spatial threshold of 100 km. The biases are about 0.2, 0.3, 0.4, 0.2, and −0.2 K for channels 10–14, respectively. The uncertainty of the bias generally increases from about 0.02 K for channel 10 to about 0.07 K for channel 14. The increase in uncertainty is related to higher NEΔT for the upper channels of ATMS (see Table I). In addition, the GPS-RO profiles only extend up to around 30 km, and the accuracy of the observations above 25 km is also questionable, which may introduce a random error in the simulations. We expected a larger bias for the upper channels, e.g., channels 13 and 14, because the vertical coverage of GPS profiles does not completely cover the entire layer where those channels are sensitive to, but the bias increases from channels 10 to 12 and then decreases. This may be because the incomplete GPS-RO profiles only introduce a random error in the simulations rather than a systematic bias. Our results are consistent with those of Zou *et al.* [38], who reported less than 0.5-K bias for ATMS channels 10–13, compared with GPS-RO data, with the largest bias for channel 12. They used a temporal threshold of 3 h and a spatial threshold of 50 km. Although we used a smaller temporal threshold, since the statistics are not affected by the collocation thresholds, the consistency between our findings and those of Zou *et al.* [38] was expected.

Fig. 10 shows the scatterplots of the ATMS observations versus the Tbs simulated using GPS-RO observations. The left column shows the scatterplots for the collocation thresholds of 30 min and 50 km and the right column for 60 min and 100 km. Although both thresholds yield a very good agreement between the simulated and observed Tbs, in general, the standard deviation is slightly larger for the scatterplots on the right side. The rows from top to bottom are for channels 10–14, and as shown, the agreement (standard deviation) decreases (increases) from channel 10 to channel 14. As aforementioned, the increase in standard deviation is mainly related to a higher

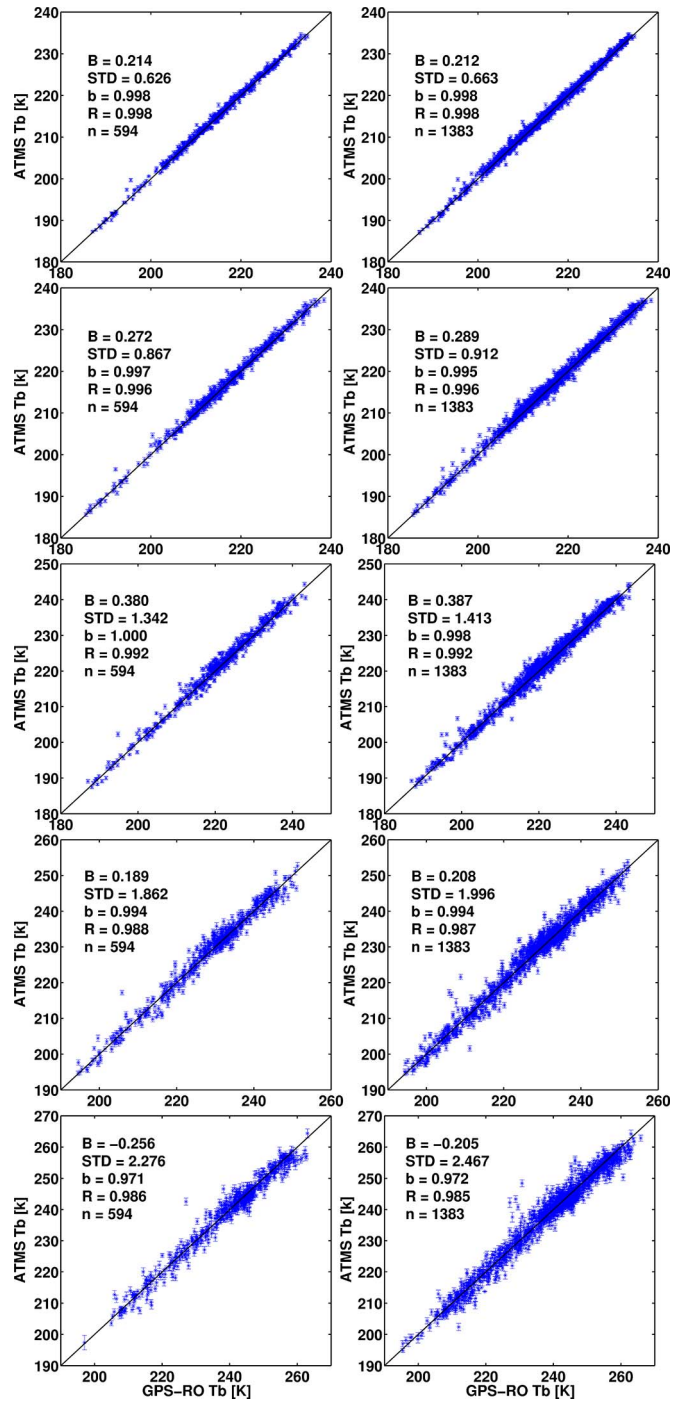

Fig. 10. ATMS Tbs versus Tbs simulated using GPS-RO profiles. The rows from top to bottom are for channels 10–14. The temporal and spatial thresholds were 50 km and 30 min for the left column and 100 km and 60 min for the right column. B indicates the bias in kelvins, STD indicates the standard deviation of the differences between the simulated and observed Tbs, b indicates the slope of the fitted line, R indicates the correlation coefficient, and n indicates the number of data points.

NEΔT for the upper temperature sounding channels of ATMS. The standard deviations shown in Fig. 10 are comparable with the NEΔT values reported in Table I. The results do not show any nonlinearity in the ATMS calibration. The slope of the fitted line is very close to unity for all the channels and only shows small dependence between the bias and the scene temperature. The accuracy of the GPS-RO comparison is affected by the

uncertainties in RT calculations, as well as sampling error due to spatial and temporal mismatch. Although it is very difficult to quantify the error in the Tbs simulated using GPS-RO, the overall error is expected to be small in a layer extending from about 5 km to about 25 km. Therefore, the GPS-RO observations provide a good opportunity for validating observations from temperature sounding channels that are sensitive to this layer, e.g., channels 10 and 11. Although the error increases toward the lower troposphere and the upper stratosphere, nevertheless, the GPS-RO comparison can be used to identify the overall accuracy of the observations from channels 9 and 12–14.

V. Conclusion

MW satellite data from the SAPHIR and ATMS instruments are crucial to derive a variety of hydrological and meteorological products such as temperature, humidity, precipitation, and cloud physical parameters. In this paper, these instruments have been intercompared and validated using radiosonde and GPS-RO observations. The results show that the systematic differences between the observations from the two instruments are very small relative to the instrument noise and that, in general, the data from the two instruments are in a very good agreement. The SAPHIR data showed a small systematic negative difference relative to the ATMS data, but further analysis using coincident data from SAPHIR and MHS showed that this systematic difference should not be interpreted as either a cold bias in the SAPHIR data or a warm bias in the ATMS data.

The ATMS temperature sounding channels sensitive to upper troposphere and stratosphere were validated using GPS-RO profiles. The mean difference between the GPS-RO and ATMS observations ranges between -0.2 and 0.4 K, and the statistical uncertainty of the bias varies from 0.02 K for channel 10 to about 0.07 K for channel 14. The larger uncertainties for the upper level channels are introduced by a higher NEΔT for the ATMS upper channels, as well as lower accuracy for GPS-RO profiles at altitudes above 30 km.

Radiosonde data were used to validate ATMS middle and upper tropospheric temperature sounding channels and ATMS and SAPHIR water vapor channels. The bias was generally larger for the water vapor channels, which is related to error in the radiosonde humidity measurements.

It should be noted that the cross calibration of satellite data can only reveal the relative difference between the two instruments. Validating satellite data using atmospheric profiles from radiosonde and GPS profiles is an alternative method to independently evaluate the accuracy of the observations. The difference between observed and simulated Tbs is affected by several errors, including bias in the temperature and humidity profiles, error in RT calculations, and sampling errors due to time difference and spatial distance between the collocations. Nevertheless, GPS-RO and radiosonde data provide a good opportunity for independent evaluation of satellite observations.

Acknowledgment

The views, opinions, and findings contained in this paper are those of the authors and should not be construed as an official National Oceanic and Atmospheric Administration or U.S. Government position, policy, or decision.

References

[1] R. R. Ferraro *et al.*, "NOAA operational hydrological products derived from the Advanced Microwave Sounding Unit," *IEEE Trans. Geosci. Remote Sens.*, vol. 43, no. 5, pp. 1036–1049, May 2005.

[2] S. A. Buehler *et al.*, "An upper tropospheric humidity data set from operational satellite microwave data," *J. Geophys. Res.*, vol. 113, no. D14, Jul. 2008, Art. ID. D14110.

[3] I. Moradi, S. A. Buehler, V. O. John, and S. Eliasson, "Comparing upper tropospheric humidity data from microwave satellite instruments and tropical radiosondes," *J. Geophys. Res.*, vol. 115, no. D24, Dec. 2010, Art. ID. D24310.

[4] B. J. Choudhury, "Passive microwave remote sensing contribution to hydrological variables," *Surveys Geophys.*, vol. 12, no. 1–3, pp. 63–84, Mar. 1991.

[5] H. Brogniez, P. Kirstetter, and L. Eymard, "Expected improvements in the atmospheric humidity profile retrieval using the Megha-Tropiques microwave payload," *Q. J. R. Meteorol. Soc.*, vol. 139, no. 673, pp. 842–851, Apr. 2013.

[6] I. Moradi, H. Meng, and R. Ferraro, "Correcting geolocation errors for microwave instruments aboard NOAA satellites," *IEEE Trans. Geosci. Remote Sens.*, vol. 51, no. 6, pp. 3625–3637, Jun. 2013.

[7] W. J. Blackwell, L. J. Bickmeier, L. G. Jairam, and R. V. Leslie, "On-orbit radiometric validation and field-of-view calibration of spaceborne microwave sounding instruments," in *Proc. SPIE Microw. Remote Sens. Atmos. Environ. VI*, A. Valinia, P. H. Hildebrand, and S. Uratsuka, Eds. 2008, pp. 71540A–71540A-12.

[8] T. Wilheit, "Comparing calibrations of similar conically scanning window-channel microwave radiometers," *IEEE Trans. Geosci. Remote Sens.*, vol. 51, no. 3, pp. 1453–1464, Mar. 2013.

[9] M. Sapiano, W. Berg, D. McKague, and C. Kummerow, "Toward an intercalibrated fundamental climate data record of the SSM/i sensors," *IEEE Trans. Geosci. Remote Sens.*, vol. 51, no. 3, pp. 1492–1503, Mar. 2013.

[10] V. O. John, R. P. Allan, W. Bell, S. A. Buehler, and A. Kottayil, "Assessment of intercalibration methods for satellite microwave humidity sounders," *J. Geophys. Res.*, vol. 118, no. 10, pp. 4906–4918, May 2013.

[11] W. Blackwell *et al.*, "Radiometer calibration using collocated GPS radio occultation measurements," *IEEE Trans. Geosci. Remote Sens.*, vol. 52, no. 10, pp. 6423–6433, Oct. 2014.

[12] W. Blackwell *et al.*, "NPP ATMS prelaunch performance assessment and sensor data record validation," in *Proc. IEEE IGARSS*, Jul. 2011, pp. 32–34.

[13] E. Kim, C.-H. J. Lyu, K. Anderson, R. Vincent Leslie, and W. J. Blackwell, "S-NPP ATMS instrument prelaunch and on-orbit performance evaluation," *J. Geophys. Res.*, vol. 119, no. 9, pp. 5653–5670, May 2014.

[14] M. Venkat Ratnam, G. Basha, B. V. Krishna Murthy, and A. Jayaraman, "Relative humidity distribution from SAPHIR experiment onboard Megha-Tropiques satellite mission: Comparison with global radiosonde and other satellite and reanalysis data sets," *J. Geophys. Res. Atmos.*, vol. 118, no. 17, pp. 9622–9630, Sep. 2013.

[15] Advanced Technology Microwave Sounder (ATMS). SDR radiometric calibration. Algorithm Theoretical Basis Document (ATBD), N. Baker, Ed., Joint Polar Satellite System (JPSS) Ground Project, the National Aeronautics and Space Administration, 2011.

[16] F. Weng *et al.*, "Calibration of Suomi National Polar-orbiting Partnership advanced technology microwave sounder," *J. Geophys. Res. Atmos.*, vol. 118, no. 19, pp. 11 187–11 200, Oct. 2013.

[17] F. Weng, H. Yang, and X. Zou, "On convertibility from antenna to sensor brightness temperature for ATMS," *IEEE Geosci. Remote Sens. Lett.*, vol. 10, no. 4, pp. 771–775, Jul. 2013.

[18] E. R. Kursinski, G. A. Hajj, J. T. Schofield, R. P. Linfield, and K. R. Hardy, "Observing Earth's atmosphere with radio occultation measurements using the global positioning system," *J. Geophys. Res.*, vol. 102, no. D19, pp. 23 429–23 465, Oct. 1997.

[19] C. O. Ao, A. J. Mannucci, and E. R. Kursinski, "Improving GPS radio occultation stratospheric refractivity retrievals for climate benchmarking," *Geophys. Res. Lett.*, vol. 39, no. 12, Jun. 2012, Art. ID. L12701.

[20] S.-P. Ho *et al.*, "Reproducibility of GPS radio occultation data for climate monitoring: Profile-to-profile inter-comparison of CHAMP climate records 2002 to 2008 from six data centers," *J. Geophys. Res.*, vol. 117, no. D18, Sep. 2012, Art. ID. D18111.

[21] S. Sokolovskiy, "Effect of superrefraction on inversions of radio occultation signals in the lower troposphere," *Radio Sci.*, vol. 38, no. 3, pp. 1058–1072, Jun. 2003.

[22] C. O. Ao, T. K. Meehan, G. A. Hajj, A. J. Mannucci, and G. Beyerle, "Lower troposphere refractivity bias in GPS occultation retrievals," *J. Geophys. Res.*, vol. 108, no. D18, pp. 4577–4593, Sep. 2003.

[23] B. Ahmad and G. L. Tyler, "Systematic errors in atmospheric profiles obtained from Abelian inversion of radio occultation data: Effects of large-scale horizontal gradients," *J. Geophys. Res.*, vol. 104, no. D4, pp. 3971–3992, Feb. 1999.
[24] G. M. Stokes and S. E. Schwartz, "The Atmospheric Radiation Measurement (ARM) program: Programmatic background and design of the cloud and radiation test bed," *Bull. Amer. Meteorol. Soc.*, vol. 75, no. 7, pp. 1201–1221, Jul. 1994.
[25] C. N. Long *et al.*, "ARM research in the equatorial western pacific: A decade and counting," *Bull. Amer. Meteorol. Soc.*, vol. 94, no. 5, pp. 695–708, May 2013.
[26] I. Moradi, B. Soden, R. Ferraro, P. Arkin, and H. Vömel, "Assessing the quality of humidity measurements from global operational radiosonde sensors," *J. Geophys. Res.*, vol. 118, no. 14, pp. 8040–8053, Jul. 2013.
[27] H. Vömel *et al.*, "Radiation dry bias of the Vaisala RS92 humidity sensor," *J. Atmos. Ocean. Technol.*, vol. 24, no. 6, pp. 953–963, Jun. 2007.
[28] Q. Liu *et al.*, "Community radiative transfer model for radiance assimilation and applications," in *Proc. IEEE IGARSS*, 2012, pp. 3700–3703.
[29] B. Burns, X. Wu, and G. Diak, "Effects of precipitation and cloud ice on brightness temperatures in AMSU moisture channels," *IEEE Trans. Geosci. Remote Sens.*, vol. 35, no. 6, pp. 1429–1437, Nov. 1997.
[30] R. F. Adler, R. A. Mack, N. Prasad, H. Y. M. Yeh, and I. M. Hakkarinen, "Aircraft microwave observations and simulations of deep convection from 18 to 183 GHz—Part I: Observations," *J. Atmos. Ocean. Technol.*, vol. 7, no. 3, pp. 377–391, Jun. 1990.
[31] S. A. Buehler *et al.*, "A cloud filtering method for microwave upper tropospheric humidity measurements," *Atmos. Chem. Phys.*, vol. 7, no. 21, pp. 5531–5542, Nov. 2007.
[32] E.-K. Seo and G. Liu, "Retrievals of cloud ice water path by combining ground cloud radar and satellite high-frequency microwave measurements near the ARM SGP site," *J. Geophys. Res.*, vol. 110, no. D14, Jul. 2005, Art. ID. D14203.
[33] S. D. Michele and P. Bauer, "Passive microwave radiometer channel selection based on cloud and precipitation information content," *Q. J. R. Meteorol. Soc.*, vol. 132, no. 617, pp. 1299–1323, Apr. 2006.
[34] G. Clain, H. Brogniez, V. H. Payne, V. O. John, and M. Luo, "An assessment of SAPHIR calibration using quality tropical soundings," *J. Atmos. Ocean. Technol.*, vol. 32, no. 1, pp. 61–78, Jan. 2015.
[35] W. P. Elliott and D. J. Gaffen, "On the utility of radiosonde humidity archives for climate studies," *Bull. Amer. Meteorol. Soc.*, vol. 72, no. 10, pp. 1507–1520, Oct. 1991.
[36] L. M. Miloshevich *et al.*, "Absolute accuracy of water vapor measurements from six operational radiosonde types launched during AWEX-G and implications for AIRS validation," *J. Geophys. Res.*, vol. 111, no. D9, May 2006, Art. ID. D09S10.
[37] L. M. Miloshevich, H. Vömel, D. N. Whiteman, and T. Leblanc, "Accuracy assessment and correction of Vaisala RS92 radiosonde water vapor measurements," *J. Geophys. Res.*, vol. 114, no. D11, Jun. 2009, Art. ID. D11305.
[38] X. Zou, L. Lin, and F. Weng, "Absolute calibration of ATMS upper level temperature sounding channels using GPS RO observations," *IEEE Trans. Geosci. Remote Sens.*, vol. 52, no. 2, pp. 1397–1406, Feb. 2014.
[39] M. T. Team, "Megha-Tropiques level 1 products definition," CNES, Paris, France, 2013.

Isaac Moradi received the M.Sc. degree in meteorology from the University of Tehran, Tehran, Iran, the Ph.D. degree in climatology and environmental planning from Kharazmi University, Tehran, and the Ph.D. degree in radio and space science from the Chalmers University of Technology, Gothenburg, Sweden.

He is currently with the Cooperative Institute for Climate and Satellites, Earth System Science Interdisciplinary Center, University of Maryland, College Park, MD, USA. He is also with the Joint Center for Satellite Data Assimilation, National Oceanic and Atmospheric Administration, College Park. His current activities include satellite data assimilation and developing OSSE data for different practices particularly data assimilation, calibration and validation of satellite observations, and microwave radiative transfer modeling. His other research interests include retrieving geophysical variables from microwave satellite data, solar radiation resource assessment, and developing new sensor concepts, particularly for measuring tropospheric humidity.

Ralph R. Ferraro received the B.S. degree in meteorology from Rutgers University, New Brunswick, NJ, USA, and the M.S. degree in meteorology from the University of Maryland, College Park, MD, USA.

He is currently the Chief of the Satellite Climate Studies Branch, National Environmental Satellite, Data, and Information Service, National Oceanic and Atmospheric Administration, College Park. His research interests include the use of passive microwave sensors to retrieve parameters related to the hydrological cycle.

Patrick Eriksson graduated in engineering physics and the Ph.D. degree in environmental sciences from Chalmers University of Technology, Gothenburg, Sweden, in 1990 and 1999, respectively.

He is currently a Professor of global environmental measurements at the same university. His main areas of expertise are atmospheric radiative transfer and retrieval methodologies, with a focus on passive microwave sounding of the atmosphere. For example, he is a core member of the team around the submillimeter radiometer on board the Odin satellite. He and Stefan Buehler (University of Hamburg) are leading the development of the Atmospheric Radiative Transfer System (ARTS) open-source software. Based on ARTS, he has implemented a general inversion package (Qpack), used, for example, by several groups operating ground-based receivers. The present research is directed toward atmospheric water, in both gas and ice phase, between 5 and 100 km.

Fuzhong Weng received the Ph.D. degree from Colorado State University, Fort Collins, CO, USA, in 1992.

He is currently the Chief of the Satellite Meteorology and Climatology Division, Center for Satellite Applications and Research, National Environmental Satellite, Data, and Information Service; a Senior Scientist of the Joint Center for Satellite Data Assimilation; and a Joint Polar Satellite System Sensor Science Chair with NOAA, College Park, MD, USA. He is a leading expert in satellite instrument calibration, radiative transfer theory and modeling, satellite products developments, applications of satellite data in weather and climate prediction models, and satellite data assimilation. He has authored or coauthored over 130 papers in American journals (e.g., American Meteorological Society, American Geophysical Union, and IEEE) and other international journals.

Dr. Weng was the first winner of the 2000 NOAA David Johnson Award for his outstanding contributions to satellite microwave remote sensing fields and the utilization of satellite data in the NWP models and a recipient of the U.S. Department of Commerce Gold Medal Award in 2005 for his achievement in satellite data assimilation and the NOAA bronze medal for leading successful NOAA-18 instrument calibration. He has been also a recipient of the NOAA Administrator's Award for developing new and powerful radiative transfer models to assimilate advanced satellite data.